DYNAMICS OF GALAXIES

5. Observations of distributions

Piet van der Kruit
Kapteyn Astronomical Institute
University of Groningen
the Netherlands

Winter 2008/9

Outline

Stellar Populations

Origin of the concept

Lindblad[1] in 1925 argued that the Galaxy is made up of a set of components with a continuous range of flattening.

Baade[2] in 1944 resolved red stars in the central regions of M32 and the elliptical companions and introduces the concept of two stellar populations, mainly based on the characteristics of their H-R diagrams. Population I is in the disk and has blue stars and

Population II in the halo with globular cluster type H-R diagrams with red stars the brightest.

---

[1] B. Lindblad, Arkiv. Mat. Astron. Fysik 19A, No. 21 (1925)
[2] W. Baade, Ap.J. 100, 137 and 147 (1944)

THE RESOLUTION OF MESSIER 32, NGC 205, AND THE CENTRAL REGION OF THE ANDROMEDA NEBULA*

W. BAADE
Mount Wilson Observatory
Received April 27, 1944

ABSTRACT

Recent photographs on red-sensitive plates, taken with the 100-inch telescope, have for the first time resolved into stars the two companions of the Andromeda nebula—Messier 32 and NGC 205—and the central region of the Andromeda nebula itself. The brightest stars in all three systems have the photographic magnitude 21.3 and the mean color index +1.3 mag. Since the revised distance-modulus of the group is $m - M = 22.4$, the absolute photographic magnitude of the brightest stars in these systems is $M_{pg} = -1.1$.

The Hertzsprung-Russell diagram of the stars in the early-type nebulae is shown to be closely related to, if not identical with, that of the globular clusters. This leads to the further conclusion that the stellar populations of the galaxies fall into two distinct groups, one represented by the well-known H-R diagram of the stars in our solar neighborhood (the slow-moving stars), the other by that of the globular clusters. Characteristic of the first group (type I) are highly luminous O- and B-type stars and open clusters; of the second (type II), short-period Cepheids and globular clusters. Early-type nebulae (E–Sa) seem to have populations of the pure type II. Both types seem to coexist in the intermediate and late-type nebulae.

The two types of stellar populations had been recognized among the stars of our own galaxy by Oort as early as 1926.

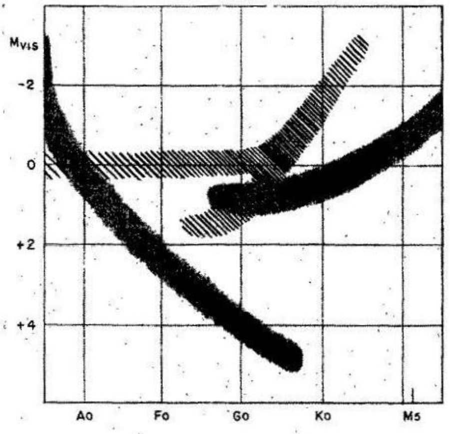

FIG. 1.—Shaded areas: ordinary H-R diagram (type I). Hatched area: H-R diagram of stars in globular clusters (type II).

The Galaxy as consisting of two basic populations can be seen in the distribution on the sky of globular (red) versus galactic clusters.

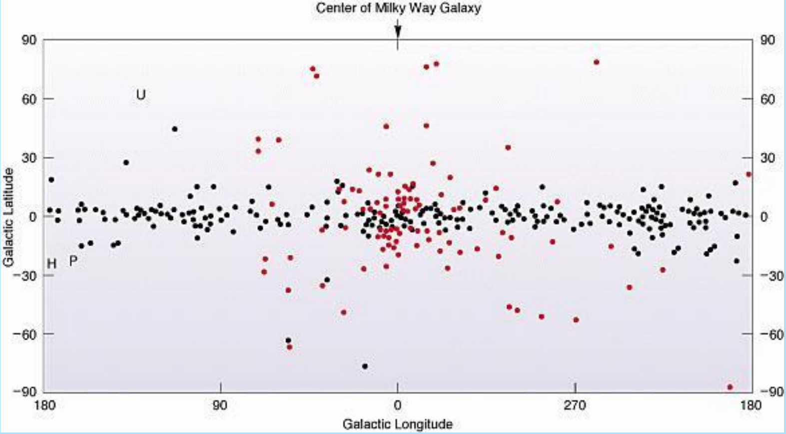

and in the near-infrared image of the Galaxy with the DIRBE experiment on board the Cosmic Background Explorer COBE.

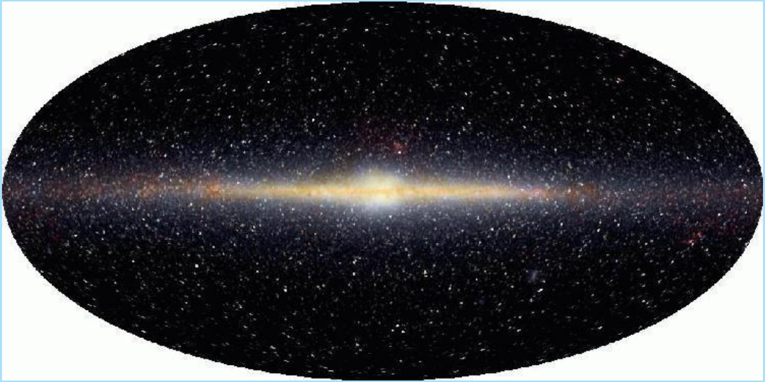

Vatican Symposium

In 1957 the Vatican Symposium on stellar populations defined five stellar populations with a decreasing age, increasing flattening and metal abundance.

Population	$\lvert z \rvert$ (pc)	$\lvert Z \rvert$ (km/s)	Typical members
Extreme Pop. I	120	8	Gas, Young stars associated with spiral structure, Supergiants, Cepheids, T Tauri stars, Galactic Clusters of Trumpler's Class I
Older Pop. I	160	10	A-Type stars, Strong-line stars
Disk Population	400	17	Stars of galactic nucleus, Planetary Nebulae, novae, RR Lyrae stars with periods below 0.4 days, Weak-line stars
Interm. Pop. II	700	25	"High-velocity stars" with z-velocities exceeding 30 km/sec, Long-period variables <M5e with periods below 250 days
Halo Pop. II	2000	75	Subdwarfs, Globular clusters with high z-velocity, RR Lyrae stars with periods longer than 0.4 days

The current situation.

- Dark halo, presumably non-baryonic.
- Population II.
- Thick disk.
- Old disk, sometimes called thin disk.
- Population I.

Classification

frame

Definition by Hubble and later extensions

Classification systems have been described in detail by Allan Sandage in Volume IX of “Stars and Stellar Systems”[3].

The Hubble classification scheme starts with Hubble's scheme of the 1920's (his well-known tuning fork).

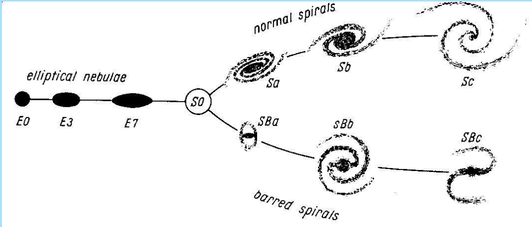

Originally the S0 class was not included. Hubble introduced it in the 1930's.

Here is a modern WWW-version of the Tuning Fork.

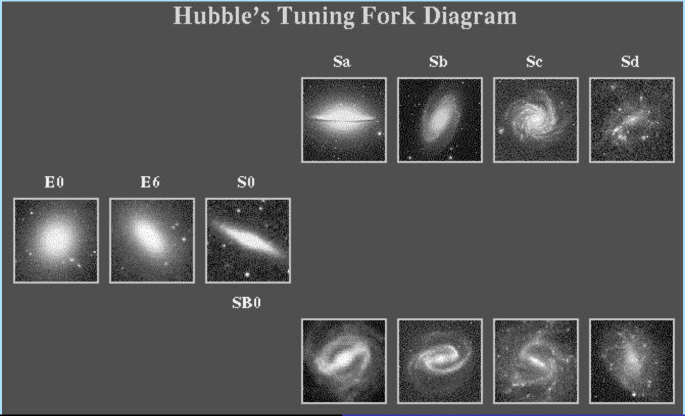

The Hubble Classification System has the following criteria:

- Ellipticals – E0 to E7 depending on the apparent flattening (En with $n = 10 \times (a - b)/a$).
- Spirals either with or without a bar S or SB) and subclasses a to c depending on
  - Bulge-to-disk ratio
  - Pitch angle of spiral arms
  - Development of arms ("strength" of HII regions)
- Irregulars Irr

A set of pictures of edge-on galaxies along the Hubble sequence.

Correlations along the Hubble sequence

Hubble classification correlates with integrated colors[4] and relative HI content[5], so is apparantly related to the history of star formation.

The colors of E-galaxies are about $(B-V)\sim 0.9$, $(U-B)\sim 0.6$ and those for late type galaxies $(B-V)\sim 0.4$, $(U-B)\sim -0.3$.

The HI content is expressed as the hydrogen mass to luminosity ratio

[4] R.B. Larson & B.M. Tinsley, Ap.J. 219, 46 (1978)
[5] M.S. Roberts, A.J. 74, 859 (1969)

The Hubble Atlas has normal galaxies; the Arp Atlas has disturbed and interacting galaxies.

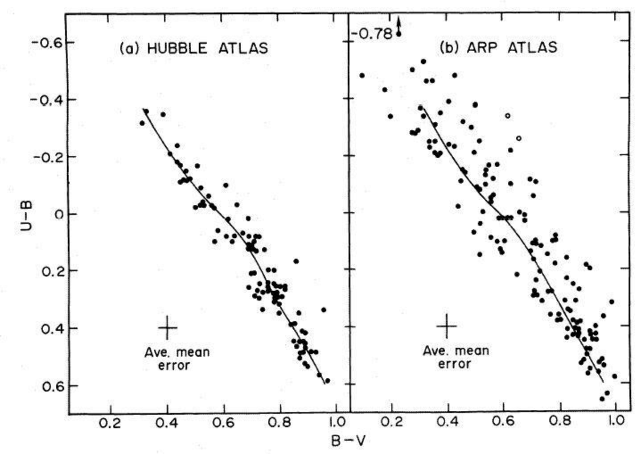

Note that both the colors and these HI/L ratios are distance independent, since both are ratios of fluxes.

It follows that the Hubble sequence is one according to the relative importance of the two fundamental populations.

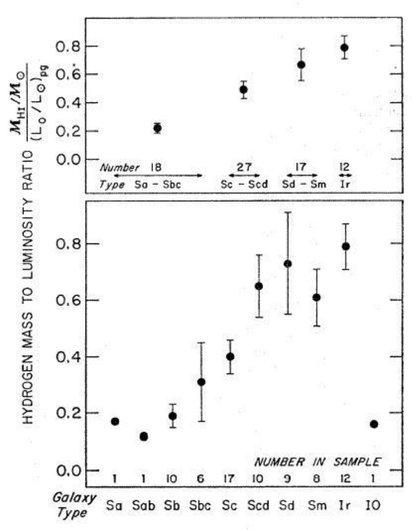

Surface photometry

Photographic surface photometry

Photographic surface photometry is mentioned only for historical interest.

It relies on the possibility to derive an accurate characteristic curve of the photographic plate.

This is done by taking on the same plate exposures of a set of spots with known intensity ratios or a continuous wedge with known intensity gradient.

This has to be done for about the same exposure time because of low intensity reciprocity failure.

The procedure of photographic surface photometry is:

- Digitize the plate. You need a machine to accurately measure the "photographic density" D over many pixels. Density is minus the logarithm of the percentage of light coming through the emulsion, so $D = 0$ means completely clear, $D = 1$ only 10%, etc.
- Determine the characteristic curve. This is the relation between D and the "exposure" E. This is the total amount of light that fell onto the emulsion.
- Fit the sky background. This is a polynomial fit to the density of sky outside the object and in between stars.
- Zero-point calibration of the magnitude scale. This must be done separately from aperture photometry (usually from the literature).

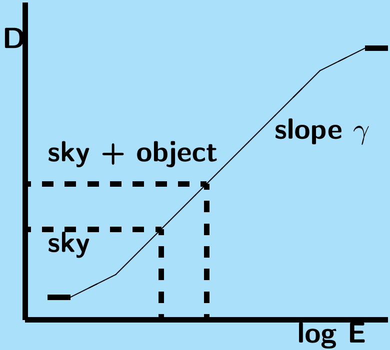

The photographic plate is a-linear and has a limited dynamic range.

Digital surface photometry.

Charge Coupled Devices (CCD's) are now the detectors used almost exclusively.

Each pixel has a number of electrons proportional (or almost equal) to the number of photons received.

The procedure of CCD surface photometry is:

- Bias subtraction. Even when not exposed, the CCD records electrons. So, you have to take separate "bias-frames" with the shutter closed.

- Remove bad pixels. These are due to cosmic rays. In practice the maximum exposure is of order half an hour. So, you take separate frames and add these later.
- Flat-fielding. Correction for sensitivity changes between pixels. For this you take an exposure on a uniformly illuminated screen in the dome or an exposure of the twilight sky.
- Sky subtraction. Fit the background sky and subtract.
- Calibration. You take frames during the same night of standard stars with known magnitudes.

Photographic plates have a large size in terms of pixels and a-linearity is not a fundamental problem.

The disadvantages of photographic plates that have been overcome by digital techniques are:

- Need to digitize.
- Low quantum efficiency (no more than 15% or so, while CCD's go up to close to 100%).
- Background non-uniformities cannot be corrected for.
- Limited dynamic range.
- Separate zero-point calibration required using aperture photometry.

Examples of surface photometry

(a.) Photographic.

This is NGC 4258[a].

The scale on the azimuthally averaged radial profile is in magnitudes per square arcsec.

For the sky this is about 22.5 at a dark site.

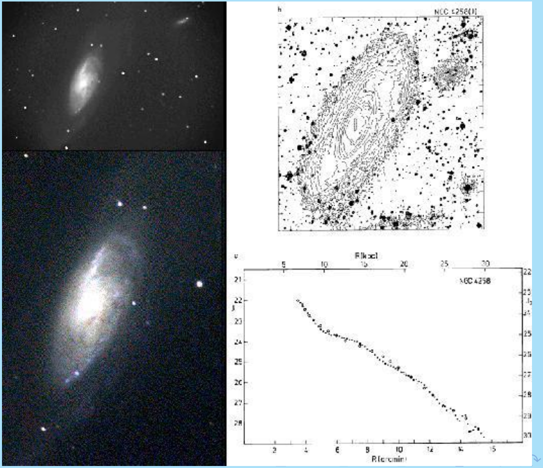

[a]P.C. van der Kruit, A.&A.Suppl. 38, 15 (1979)

(b.) CCD photometry.[6]

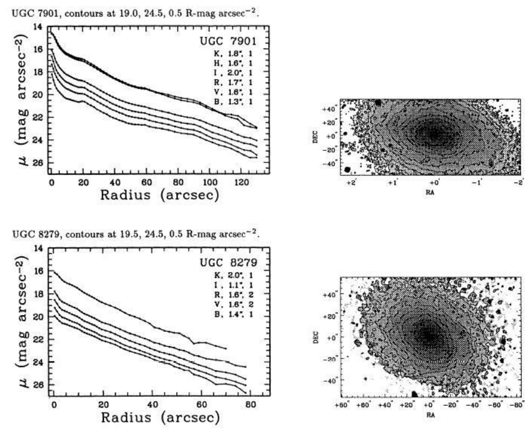

[6] R.S. de Jong & P.C. van der Kruit, A.&A.Suppl. 106, 451 (1994)

Luminosity distributions

Bulge luminosity laws

Reynolds[7] made the first fit to the M31-bulge.

He used the function:

$$(x+1)^2 y = \text{constant}$$

with x the radial distance and y the "light ratio" (relative surface brightness on a linear scale).

He went out to only 6.9 arcmin ($\sim$ 1.4 kpc). At this radius the surface brightness is 21 B-mag arcsec^{-2}.

[7] H.H.Reynolds, MNRAS. 74, 132 (1913)

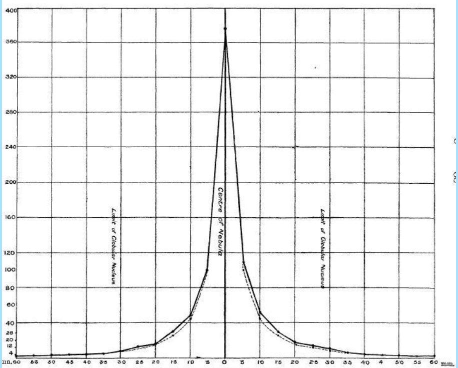

Light Curve of the Andromeda Nebula.

Hubble used this later in the form:

$$I(R) = I_0(R + a)^{-2}$$

The most commonly used fitting function is the so-called $R^{1/4}$-law found empirically by de Vaucouleurs[8].

$$\log \frac{I(R)}{I_\mathrm{e}} = -3.3307 \left[\left(\frac{R}{R_\mathrm{e}} \right)^{1/4} - 1 \right]$$

$$R_\mathrm{e} = \mathrm{Effective\ radius}$$

$$\mu(0) = \mu_\mathrm{e} + 8.3268$$

$$L = 7.215 \pi I_\mathrm{e} R_\mathrm{e}^2 (b/a)$$

[8] G. de Vaucouleurs, Ann. d'Astrophys. 11, 247 (1948)

For this there is a numerical deprojection formula from Young[9], which has an approximation for large R (in $L_\odot$ pc^{-3}):

$$L(R) = 52.19 \frac{L}{R_e^3} \left(\frac{R}{R_e} \right)^{-7/8} \cdot \exp \left[-7.67 \left(\frac{R}{R_e} \right)^{1/4} \right]$$

If flattened $R \rightarrow \alpha = \sqrt{R^2 (b/a)^2 + z^2}$.

More physical rather than empirical are the King models[10], which work best for globular clusters and also better for elliptical galaxies than bulges.

[9] P.J. Young, A.J. 81, 807 (1976)
[10] I. King, A.J. 71, 64 (1966)

They are based on isothermal distributions with upper limits on the energy of the particles and are therefore isothermal spheres with a tidal radius.

Jarvis & Freeman[11] introduce also rotation and study the effects of the gravitational effects of the disk.

The starting point is a distribution function, which is a truncated Maxwellian:

$$f(E,J) = \alpha[\exp(-\beta E) - \exp(\beta E_0)]\exp(\gamma J)$$

$E \leq E_0$ is the energy per unit mass and J the angular momentum parallel to the symmetry axis.
For $\gamma = 0$ we get the King models.

[11] B. Jarvis & K.C. Freeman, Ap.J. 295, 314 and 324 (1986)

Jarvis and Freeman take a constant M/L and include effects of disk potential, and are able to reproduce observations of both isophotes and (stellar) kinematics.

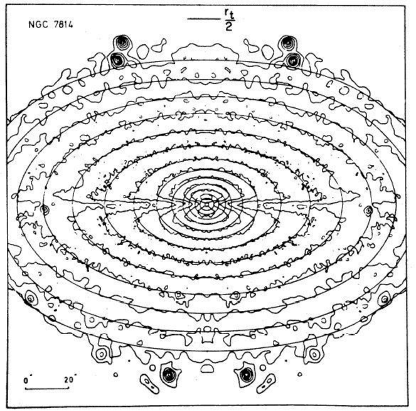

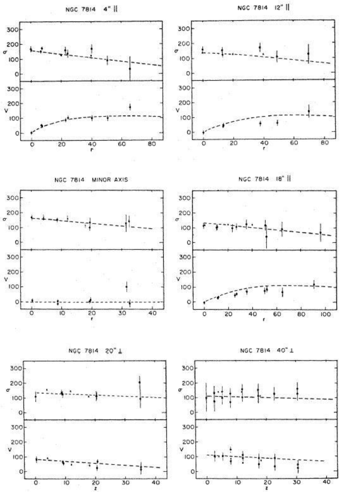

The conclusion is that bulges are consistent with isotropic, oblate spheroids, flattened mostly by rotation.

Luminosity distributions in disks

De Vaucouleurs[12] discovered that radial surface brightness profiles of disks are exponential.

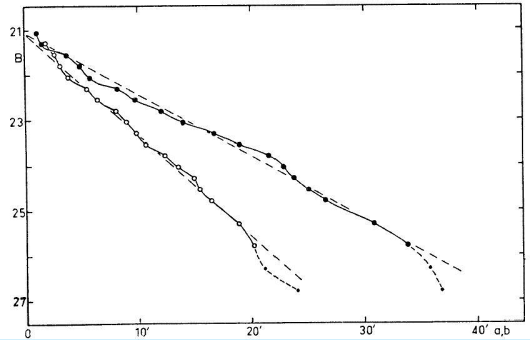

[12] G. de Vaucouleurs, Ap.J. 130, 728 (1959)

A famous paper on exponential disks and the corresponding dynamics is by Freeman[13].
The surface brightness is

$$I(R) = I_0 \exp\left(-R/h\right)$$

in linear units ($L_\odot\ \mathrm{pc}^{-2}$).

In magnitudes arcsec^{-2} it is a straight line.

The total luminosity is

$$L = 2\pi h^2 I_0$$

[13] K.C. Freeman, Ap.J. 160, 811 (1970)

Vertical distributions can (away from the dust lane) of the old disk population be approximated with an isothermal sheet.

This is not unreasonable in view of the Age - Velocity dispersion relation[a] of stars in the solar neighborhood.

Star older then a few Gyr have dispersions of the order 50 km sec^{-1}.

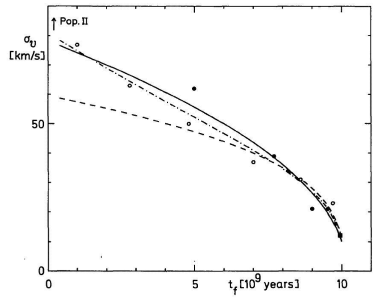

[a] R. Wielen, A.&A. 60, 263 (1977)

With the HIPPARCOS astrometric satellite better data are possible.

Here is a more recent version of the relation.[a]

[a] H. J. Rocha-Pinto et al. A.&A. 423, 517 (2004)

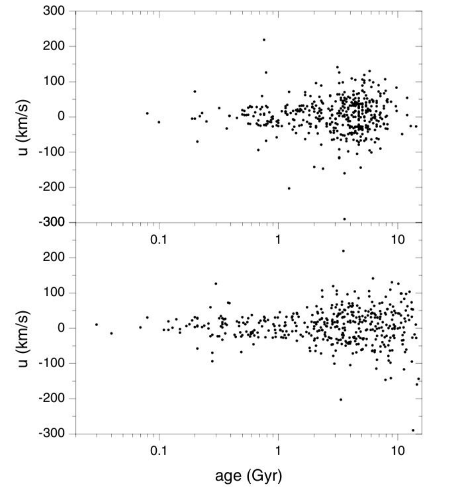

Increase of the u peculiar velocity with age, for uncorrected and corrected chromospheric ages.

The three-dimensional distribution of stars in disks was therefore proposed[14] (with the inclusion of a cut-off radius, so that $R < R_{\rm max}$) as

$$L(R,z) = L(0,0)\exp\left(-R/h\right)\,\mathrm{sech}^2(z/z_0)$$

$$I(R) = 2z_0 L(0,0)\exp\left(-R/h\right)$$

$$\langle V_z^2\rangle = \pi G I(R) z_0 (M/L)$$

[14] P.C. van der Kruit & L. Searle, A.&A. 95, 105 (1981)

For large z-distances:

$$z/z_0 \gg 1 \ \ \text{then} \ \ \ \mathrm{sech}^{\,2}(z/z_0) = 4\,\exp\,(-2z/z_0)$$

Near the plane:

$$z/z_0 \ll 1 \ \ \text{then} \ \ \ \mathrm{sech}^{\,2}(z/z_0) = \ \exp\,(-z^2/z_0^2)$$

For $R_{\max} \rightarrow \infty$:

$$I(R,z) = 2hL(0,0)(R/h)K_1(R/h)\,\mathrm{sech}^{\,2}(z/z_0)$$

Here is an isophote map of the pure disk, edge-on galaxy NGC 4244.

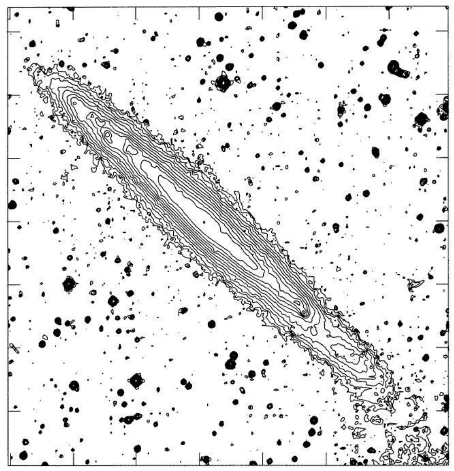

We fit profiles, averaged symmetrically, in z at various R and shifted in coincidence (left) and at a radial profile at a suitable z above the dustlane.

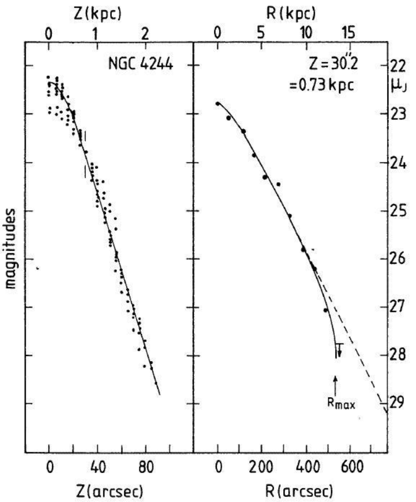

Here is the fit in directions parallel to the major axis.

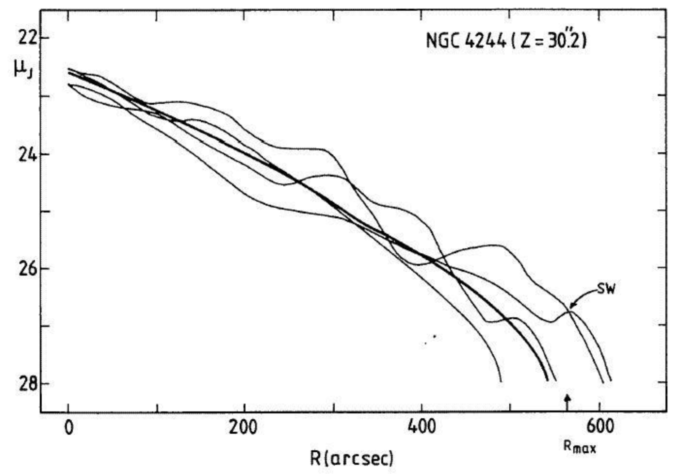

And parallel to the minor axis.

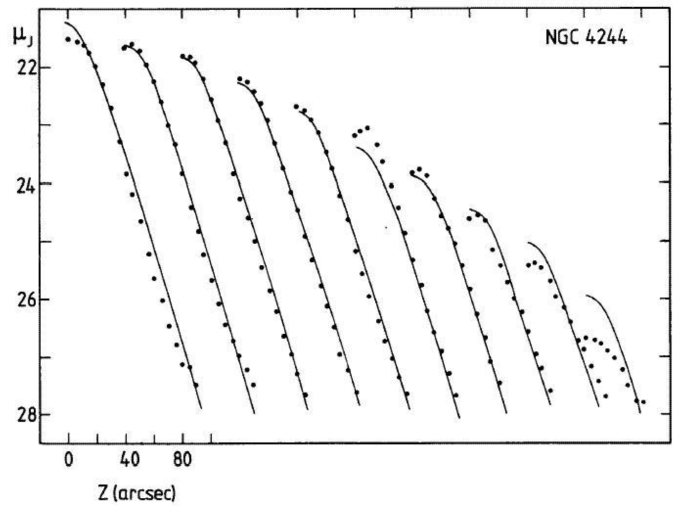

A closer look at a larger set of edge-on galaxies[15] shows that the constancy of the vertical scaleheight $z_\circ$ holds very well for late type galaxies but not for early type galaxies.

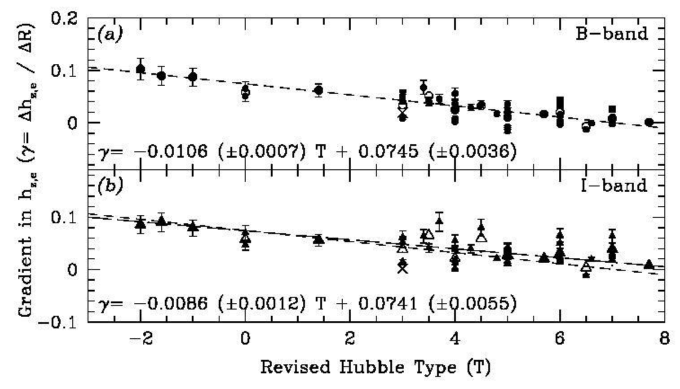

[15] R. de Grijs & R.F. Peletier, A.&A. 320, L21 (1997)

It is unlikely that at moderate and small distances above the plane the stellar population is isothermal.

Therefore a set of functions was proposed to allow for this[a]

$$L(z) = L(0)2^{-2/n}\,\mathrm{sech}^{\,2/n}\left(\frac{nz}{2z_\circ}\right)$$

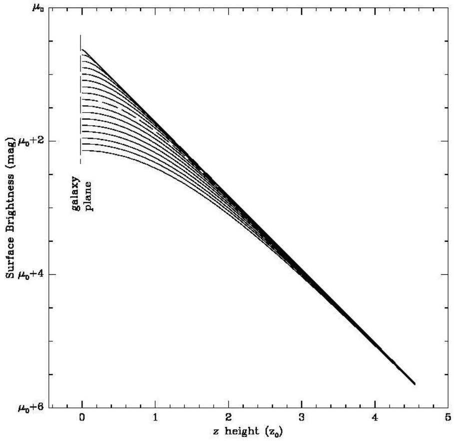

[a] P.C. van der Kruit, A.&A. 192, 117 (1988)

This ranges from the isothermal distribution for $n = 1$ to an exponential for $n = \infty$.

Fits[a] give

$$2/n = 0.54 \pm 0.20$$

in the K-band (2.2 μ).

[a] R. de Grijs, R.F. Peletier & P.C. van der Kruit, A.&A. 327, 966 (1997)

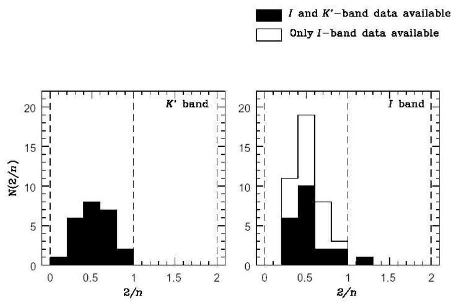

Component separation

Moderately inclined spirals

The usual assumption is to view the galaxy as built up of an exponential disk and an $R^{1/4}$-bulge.

Parameters of the fit then are:

- $\mu_{\rm e}$ and $R_{\rm e}$ for the bulge
- μ_0 and h for the disk

This is usually done with some least-squares procedure after a first guess at parameters for the dominant component.

Test on artificial images[16] show that this usually works well.

[16] J.M. Schombert & G.D. Bothun, A.J. 92, 60 (1987)

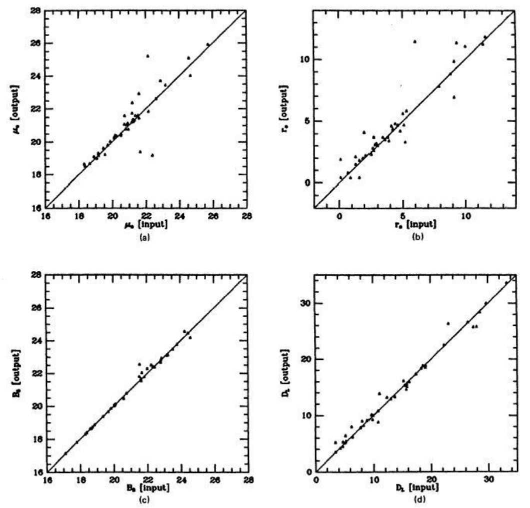

Each panel has the input parameter on the horizontal axis and the output one vertically. The top panels are for the bulge effective surface brightness and effective radius; the bottom ones are the disk central surface brightness and the scalelength.

Here are some actual component separations form Schombert & Bothun.

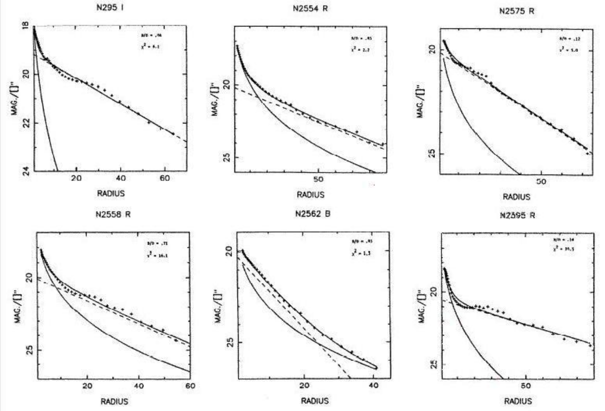

A comparison[17] of published scalelengths in the literature shows large discrepancies.

The discrepancy $d = (h_1 - h_2)/\langle h \rangle$ is plotted in the next figure as a function of $\langle h \rangle$.

The average absolute discrepancy is 23%.

This is mainly due to differences in fitting algorithms.

[17] J.H. Knapen & P.C. van der Kruit, A.&A. 248, 57 (1991)

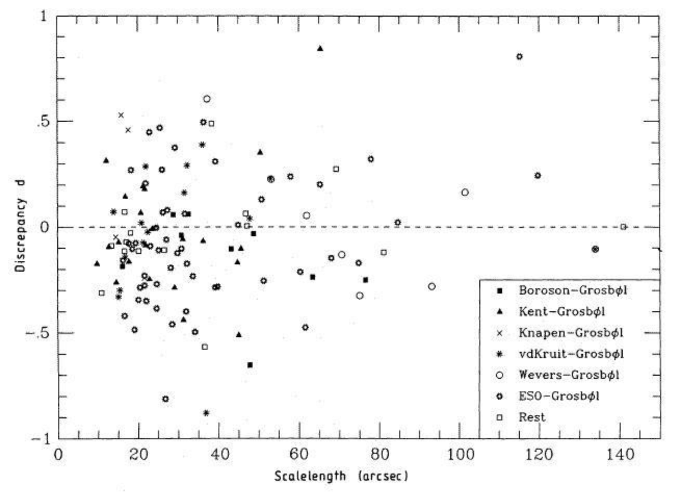
1
.5
0
−.5
−1
0
20
40
60
80
100
120
140
Discrepancy d
Scalelength (arcsec)
Boroson−Grosbøl
Kent−Grosbøl
Knapen−Grosbøl
vdKruit−Grosbøl
Wevers−Grosbøl
ESO−Grosbøl
Rest

Edge-on spirals

We now fit to a projected exponential, locally isothermal disk and an $R^{1/4}$-bulge.

Parameters of the fit now are:

- μ_0, h and z_0 for the disk
- μ_e, R_e and b/a for the bulge

The fit is made first for the dominant component and this is subtracted from the observed distribution.

We look at two examples:

NGC 891[18]. This is an Sb in which the disk dominates the light.

NGC 7814[19]. This is an Sa and the bulge dominates the light.

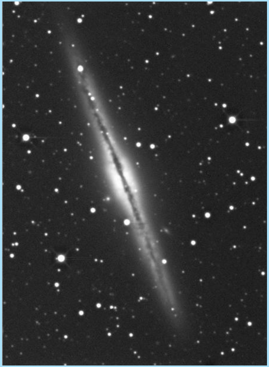

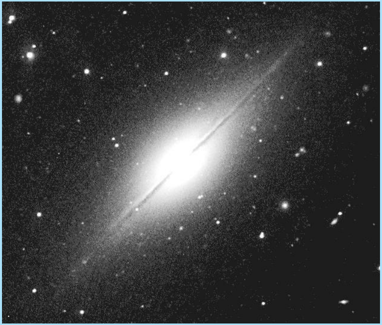

[18] van der Kruit & Searle, A.&A. 95, 116 (1981)

[19] van der Kruit & Searle, A.&A. 110, 79 (1982)

NGC 891 (D = 9.5 Mpc)

DISK (old disk only):
$L_{\rm B}(0,0) = 2.4 \times 10^{-2} L_\odot$ pc^{-3}
$h = 4.9$ kpc
$z_0 = 0.99$ kpc
$R_{\rm max} = 21$ kpc
$L = 6.7 \times 10^9 L_\odot$ (≈**82 %** of total)
$(B - V) \approx 0.8$
$(U - B) \approx 0.1$

BULGE:
$R_{\rm e} \approx 2.3$ kpc
$b/a \approx 0.6$
$L_{\rm B} \approx 1.5 \times 10^9 L_\odot$
$(B - V) \approx 0.7 \leftrightarrow 1.0$ ($6 \leftrightarrow 2$ kpc minor axis)
$(U - B) \approx -0.1 \leftrightarrow 0.4$

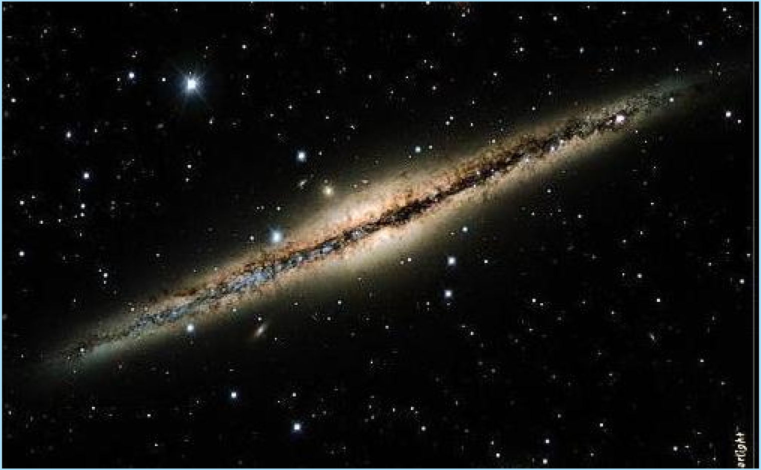

We start with the original image (here the $J \approx B$ band).

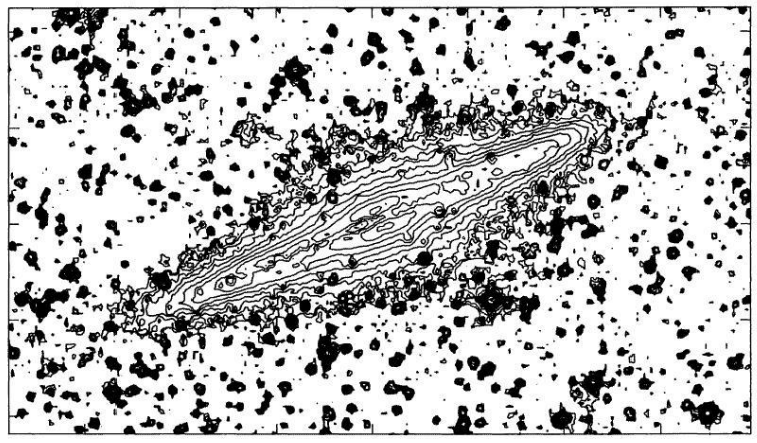

First we need to "subtract" foreground stars by interpolating over their image (or simply block them).

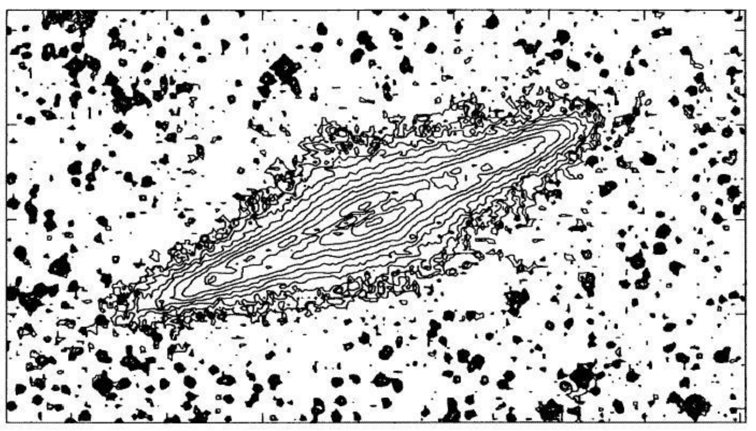

Then we make a fit for the disk from composite *R*- and *z*-profiles.

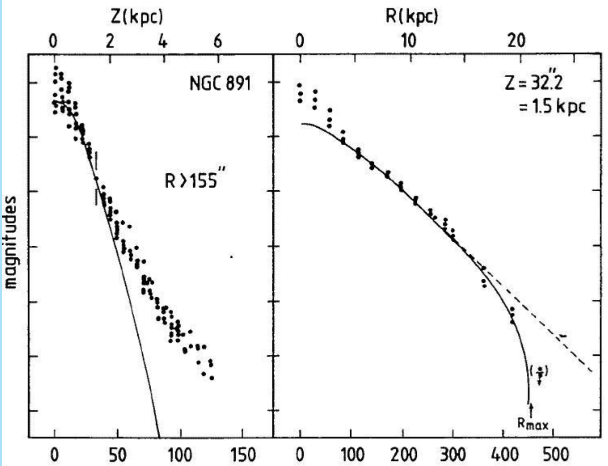

These can be checked against individual profiles. Note that we now can only fit the vertical profiles near the plane (but above the dustlane).

Here profiles parallel to the major axis.

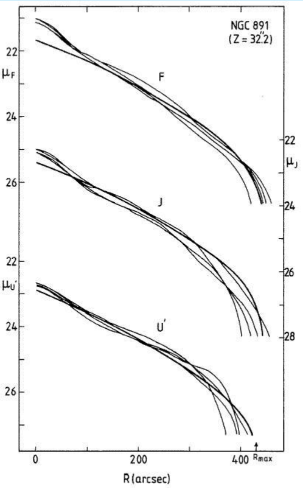

And for profiles parallel to the minor axis.

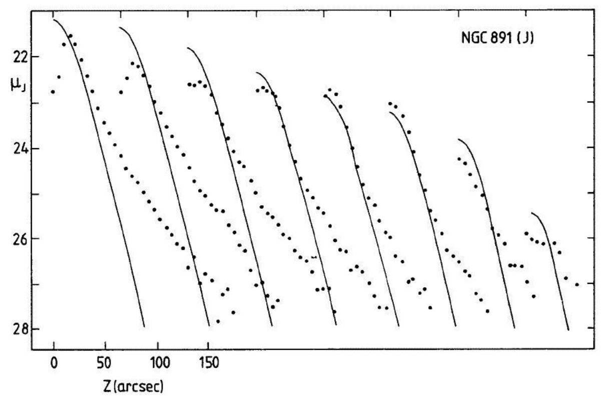

We then subtract the disk model and find the bulge brightness distribution.

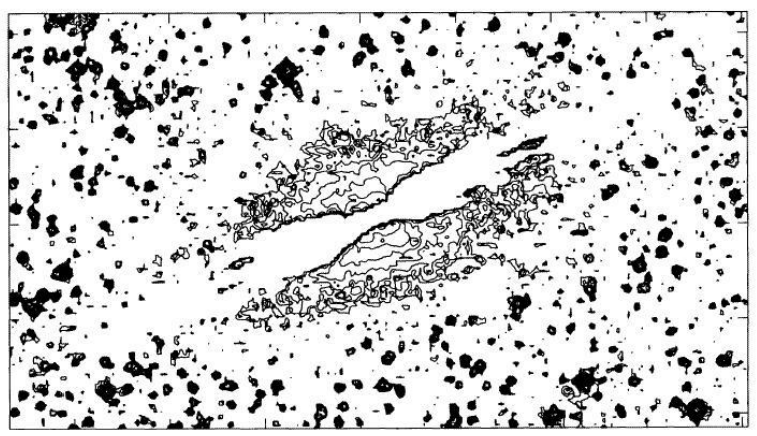

The minor axis profiles can be fitted with $R^{1/4}$ functions.

The slopes are different, so there is a color gradient (outer parts are bluer).

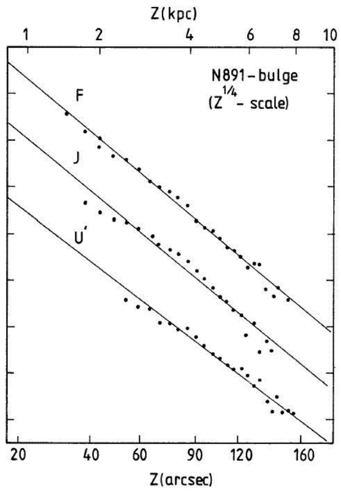

In some galaxies the stellar disks show a warping in the outer parts, such as in NGC 4565.

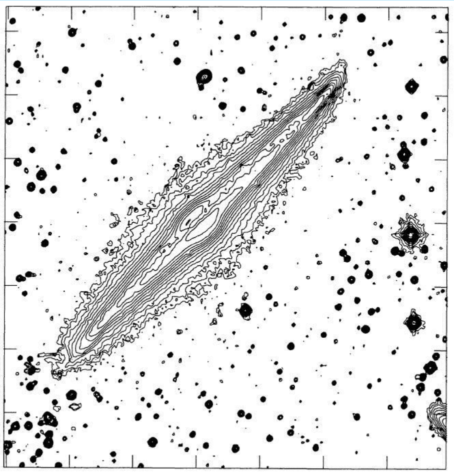

The minor axis profile cannot be fitted in this case with a single $R^{1/4}$ law.

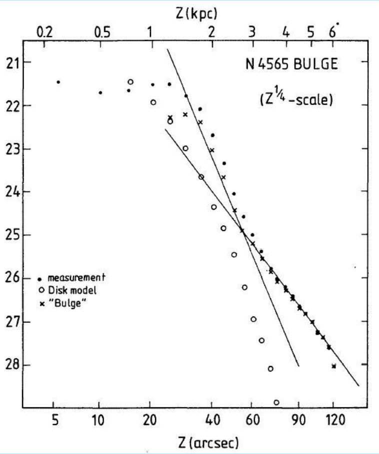

NGC 7814 (D = 15 Mpc) ,

BULGE:
$R_{\mathrm{e}} = 2.2$ kpc
$b/a = 0.57$
$L_{\mathrm{B}} = 1.6 \times 10^{10} L_{\odot}$
$(B - V) \approx 0.5 \leftrightarrow 1.3$ (13 $\leftrightarrow$ 2 kpc along minor axis)
$(U - B) \approx 0.3 \leftrightarrow 0.6$

DISK (old disk only):
$L_{\mathrm{B}}(0,0) \approx 6.6 \times 10^{-4} L_{\odot}$ pc^{-3}
$h \approx 8.4$ kpc
$z_0 \approx 2.0$ kpc
$R_{\mathrm{max}} \approx 18.2$ kpc
$L = 1.2 \times 10^{9} L_{\odot}$ ($\approx$**7 %** of total)
$(B - V) \approx 1.1$
$(U - B) \approx 0.6$

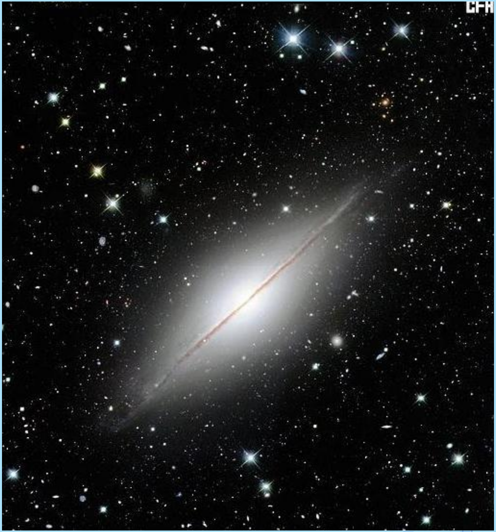

The procedure now is to find a bulge model and subtract that from the observations to reveal the disk.

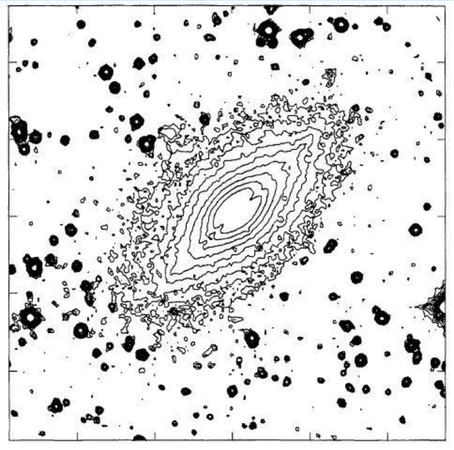

Note the bulge color gradient (bluer in the outer parts)[20] .

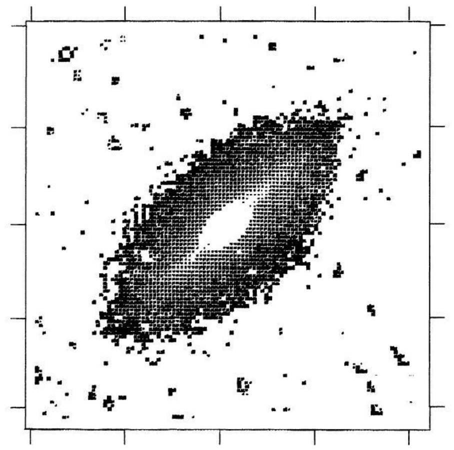

[20] See also Wainscoat, Freeman & Hyland, Ap.J. 337, 163 (1989)

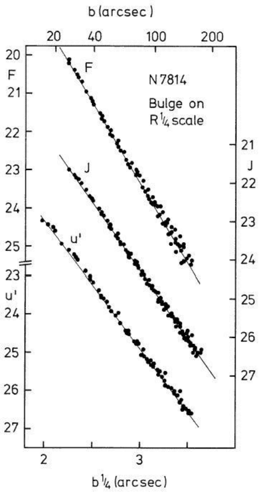

$$\mu_{U'} = 14.87 + 3.32 b^{1/4}$$
$$\mu_{J\ \mathrm{opt}} = 13.72 + 3.55 b^{1/4}$$
$$\mu_V = 13.08 + 3.75 b^{1/4}$$
$$\mu_F = 10.70 + 4.20 b^{1/4}$$
$$\mu_J = 9.19 + 4.36 b^{1/4}$$
$$\mu_K = 8.07 + 4.43 b^{1/4}$$

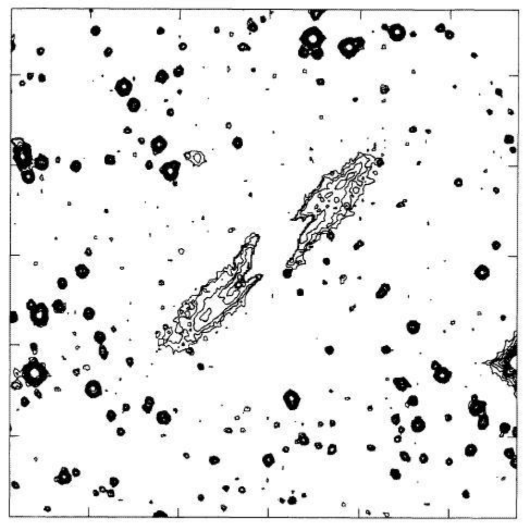

Here are some radial profiles and the fits to them.

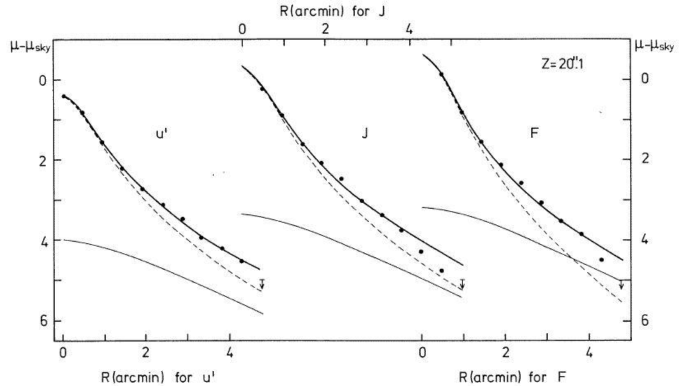

Here is the analysis in the K-Band by Wainscoat et al.

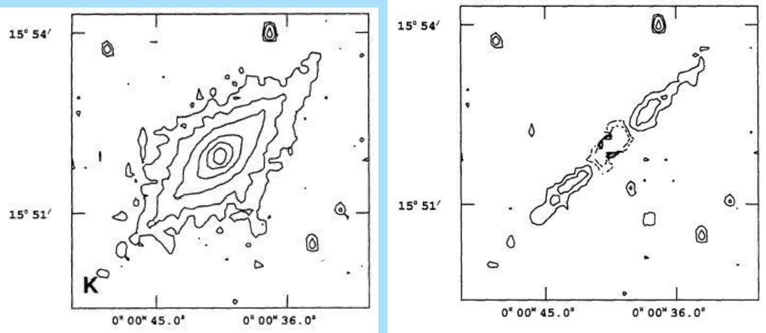

Disk truncations in face-on galaxies

In face-on or moderately inclined galaxies the disk truncations occur at faint levels. However, they can be seen as a decreasing spacing between the isophotes, as in NGC 628[21].

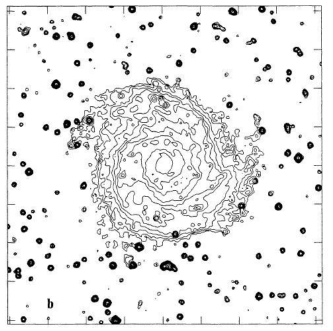

[21] P.C. van der Kruit, A.&A. 192, 117 (1988)

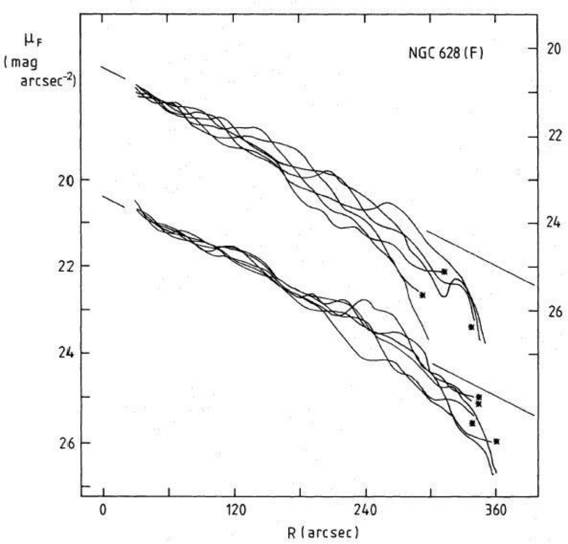
μ_F
(mag arcsec^{-2})
NGC 628 (F)
20
22
24
26
0
120
240
360
R (arcsec)

Photometric parameters

Distribution of parameters

Ken Freeman[22] was the first to study the distribution of properties of exponential disks.

His results are in the following two figures; the small range of (extrapolated) face-on, central surface brightness is known as "Freeman's Law":

$$\mu_0 = 21.67 \pm 0.30 \ \ \mathrm{B - mag\ arcsec}^{-2}$$

This has generated considerable discussion. The problem is that samples need to be statistically complete and Freeman's sample had serious selection effects.

[22] K.C. Freeman, Ap.J. 160, 811 (1970)

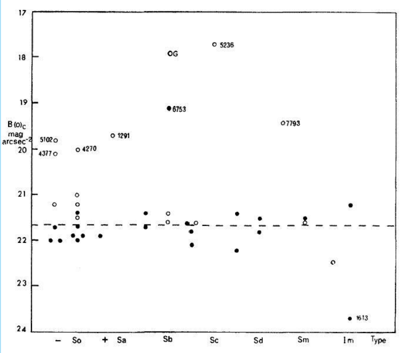
B(0)c mag arcsec-2
17
18
19
20
21
22
23
24
5102
4377
4270
1291
G
6753
5236
7793
1613
–
So
+
Sa
Sb
Sc
Sd
Sm
Im
Type

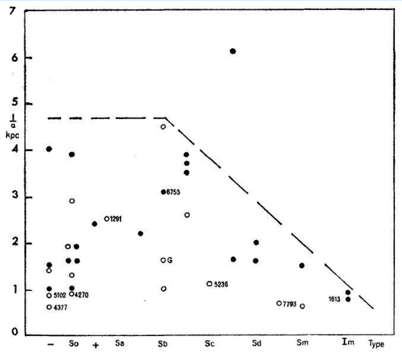
1/α kpc
7
6
5
4
3
2
1
0
5102
4377
4270
1291
6753
G
5236
7793
1613
–
So
+
Sa
Sb
Sc
Sd
Sm
Im
Type

Selection effects

The selection was discussed first by Arp [a].

We see that there is a narrow band in this diagram, excluding objects that either are have surface brightnesses that are too faint or that appear stellar.

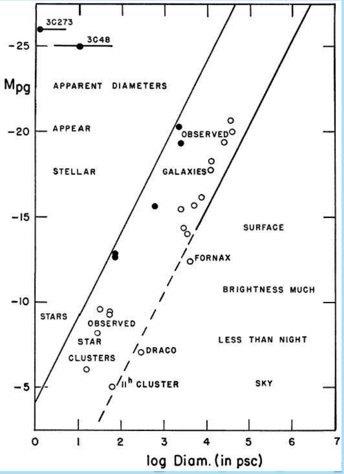

[a] H.C. Ap.J. 142, 402 (1965).

The selection effects operating here are:

- For a particular luminosity and a faint μ_0 we get a large h, but for the most part the object is fainter than sky.
- For the same luminosity and a bright μ_0 we get small h and the object will appear starlike.

We will quantify this below.

First we will consider the $V/V_{\rm max}$-test for completeness.

For this we need to know the selection criteria of the sample. These could be for example all objects down to a certain angular diameter (at some isophotal level) or integrated apparent magnitude.

Suppose that an object has a distance R. Now shift it in distance untill it drops out of the sample due to the completeness limit and call this distance $R_{\rm max}$.

Then we have V as the volume corresponding to R and $V_{\rm max}$ as the volume relating to $R_{\rm max}$.

Now, in case of a uniform space distribution each object has an uniform chance to be actually located throughout the volume $V_{\rm max}$.

In otherwords, the property $V/V_{\rm max}$ calculated for all objects in the sample should be distributed uniformly over the interval 0 to 1.

Note that $V/V_{\rm max}$ can usually be calculated without knowing the actual distance.

In practice the test is to calculate $\langle V/V_{\rm max}\rangle$. For a complete sample it is required that

$$\langle V/V_{\rm max}\rangle = 0.5.$$

The error in $\langle V/V_{\rm max}\rangle$ is $(12\ n)^{-1/2}$.

This is so, because all numbers between 0 and 1 have an average of 0.5 and a dispersion of $\sqrt{12}$.

Selection and Freeman's law

Mike Disney[23] suggested that Freeman's law is the result of sample selection.

In the process he also addressed the equivalent for elliptical galaxies, called Fish's law.

The analysis was later extended as in the following[24].

[23] M.Disney, Nature 263, 573 (1975)

[24] M. Disney & S. Phillipps, Mon.Not.R.A.S. 205, 1253 (1983); see also J.I. Davies, Mon.Not.R.A.S. 244, 8 (1990)

Assume luminosity-law (in linear units)

$$\sigma(R) = \sigma_\circ \exp \; -(R/h)^{1/b}$$

$b = 1$: exponential disk
$b = 4$: $R^{1/4}$ bulge or elliptical galaxy.

We then have for the integrated luminosity:

$$L_{\rm tot} = \int_\circ^\infty 2\pi R \sigma(R) dR = (2b)! \pi \sigma_\circ h^2$$

a. Diameter selection.

Suppose that a sample is complete for a radius larger than $\theta_{\rm lim}$ arcsec at an isophote of $\mu_{\rm lim}$ magnitudes arcsec^{-2}. For a radius R and a distance d the angular diameter is $\theta = R/d$ radians.

For clarity we now do the derivation only for an exponential disk.

The disk has an apparent radius

$$R_{\rm app} = h \ln \left(\frac{\sigma_\circ}{\sigma_{\rm lim}} \right)$$

In magnitudes arcsec^{-2} this is

$$R_{\rm app} = 0.4 \ln 10 \; h \, (\mu_{\rm lim} - \mu_\circ)$$

With $L = 2\pi\sigma_\circ h^2$ this becomes

$$R_{\rm app} = \frac{0.4 \ln 10}{\sqrt{2\pi}} \left(\frac{L}{\sigma_\circ} \right)^{-1/2} (\mu_{\rm lim} - \mu_\circ)$$

This can be rewritten as

$$R_{\rm app} \sqrt{\frac{\pi\sigma_{\rm lim}}{L}} = \frac{0.4 \ln 10}{\sqrt{2}} 10^{-0.2(\mu_{\rm lim} - \mu_\circ)} (\mu_{\rm lim} - \mu_\circ)$$

The square-root term on the lefthand side is a kind of fiducial radius, that Disney and Phillipps write as $R_{\rm L}$.

The case with $\beta = 4$ for elliptical galaxies is

$$\frac{R_{\rm app}}{R_{\rm L}} = \frac{(0.4 \ln 10)^4}{\sqrt{8!}} 10^{-0.2(\mu_{\rm lim} - \mu_\circ)} (\mu_{\rm lim} - \mu_\circ)^4$$

In the following figure we see the behavior of $R_{\rm app}/R_{\rm L}$ as a function of the central surface brightness $\mu_\circ$ for the case of a diameter selection at an isophote of 24 (B-)magnitudes arcsec^{-2}.

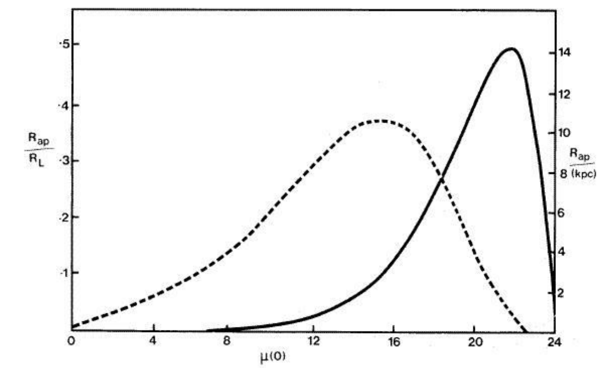

The apparent diameter for exponential disks (full line) peaks at a central surface brightness of $(\mu_{\rm lim} - \mu_\circ) = 2.171$; for elliptical galaxies (dashed line) this occurs at $(\mu_{\rm lim} - \mu_\circ) = 8.686$.

Now when we express surface brightness μ in magnitudes arcsec^{-2} and distances (such as $\sqrt{\sigma/L}$) in parsec we can derive

$$\frac{L}{\sigma_{\rm lim}} = 10^{0.4(\mu_{\rm lim} - M + 5)}$$

Then for the maximum distance for a galaxy to remain in the sample d in parsec and angular radius limit $\theta_{\rm lim}$ in arcsec we get

$$d_{\rm size} = \frac{0.4 \ln 10}{\sqrt{2\pi}} \frac{\mu_{\rm lim} - \mu_\circ}{\theta_{\rm lim}} 10^{0.2(\mu_\circ - M + 5)}.$$

For the general case the result is

$$d_{\rm size} = \frac{(0.4 \ln 10)^b}{\sqrt{\pi(2b)!}} \frac{(\mu_{\rm lim} - \mu_\circ)^b}{\theta_{\rm lim}} 10^{0.2(\mu_\circ - M + 5)}$$

The maximum of d occurs at

$$\mu_{\circ,\max} = \mu_{\rm lim} - \frac{b}{0.2 \ln 10}$$

b. Integrated magnitude selection

Now the sample is supposed complete up to a limiting integrated apparent magnitude $m_{\rm lim}$ within an isophote $\mu_{\rm lim}$.

Assume that the image is overexposed at isophote $\mu_{\rm M}$ to allow for photographic surveys and define

$$s = 0.4 \ln 10(\mu_{\rm M} - \mu_0) \;\; ; \;\; p = 0.4 \ln 10(\mu_{\rm lim} - \mu_0)$$

The maximum distance then comes out as

$$d_{\rm magn} = \left[A_{\rm s}{\rm e}^{-s} - A_{\rm p}{\rm e}^{-p}\right]^{1/2} 10^{0.2(m_{\rm lim}-M+5)}$$

with

$$A_{\rm s} = \sum_{n=0}^{n=2b} \frac{s^n}{n!} \quad ; \quad A_{\rm p} = \sum_{n=0}^{n=2b-1} \frac{p^n}{n!}$$

The following figure below is for a limiting isophote of 24 magnitues arcsec^{-2} and a saturation isophote of 19 magnitudes arcsec^{-2}.

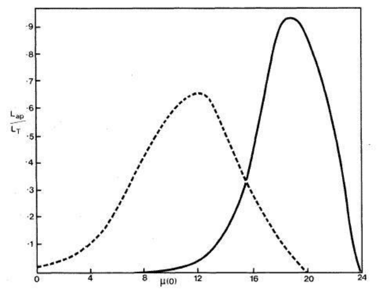

Again we see maxima as for diameter selection.

Note that both diameter and magnitude selection works in favor of disks around Freeman's surface brightness and elliptical systems near Fish's value.

Some actual values: For Palomar Sky Survey:

$\mu_{\rm lim} \approx 24$ B-mag arcsec^{-2}; $\mu_{\rm M} \approx 19$ B-mag arcsec^{-2}

Diameter selection: d^3 peaks at:
– 21.8 B-mag arcsec^{-2} for $b = 1$
– 15.3 B-mag arcsec^{-2} for $b = 4$

Magnitude selection: d^3 peaks at:
– 18.5 B-mag arcsec^{-2} for $b = 1$
– 12.0 B-mag arcsec^{-2} for $b = 4$

Observed:
$b = 1$: 21.6 ± 0.3 B-mag arcsec^{-2} (Freeman's law)
$b = 4$: 14.8 ± 0.9 B-mag arcsec^{-2} (Fish's law)

In any catalogue each galaxies has a value for d according to the selection criteria.

If both diameter and magnitude selection play a role the smalles of the two values is the appropriate one.

We can then define the visibility as the value for d^3 for each galaxy: in an unbiased sample and a uniform distribution a value of μ_0 will occur at a frequency $\propto d^3$.

The equations for the visibility can of course also be used to correct complete sample for the volumes over which galaxies are sampled as a function of their properties in order te obtain space densities as a function of parameters.

It can be used to study the question of the origin of Freeman's law and whether it results from selection effects.
Allen & Shu[25] were the first to suggest that the selection only works at the faint level and that there is only a real upper limit to the central surface brightnesses.

[25] R.J. Allen & F.H. Shu, Ap.J. 227, 67, (1979)

This is confirmed by Roelof de Jong[26], who also confirmed that the faint surface brightness disks are all of late type[27].

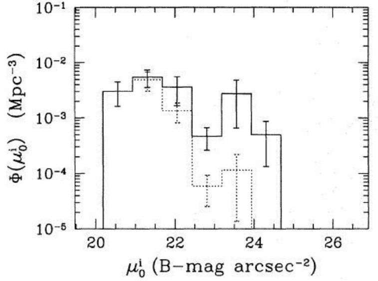

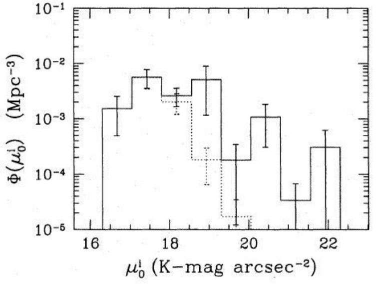

[26] R.S. de Jong, A.&A. 313, 45 (1996)
[27] P.C. van der Kruit, A.&A. 173, 59 (1987)

This is related to the fact that late type galaxies generally have fainter disks.

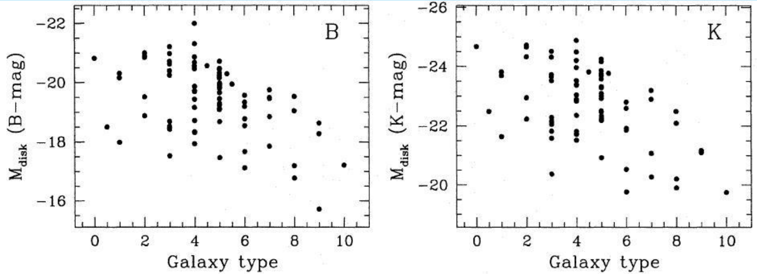

Data can be combined in bi-variate distribution functions.

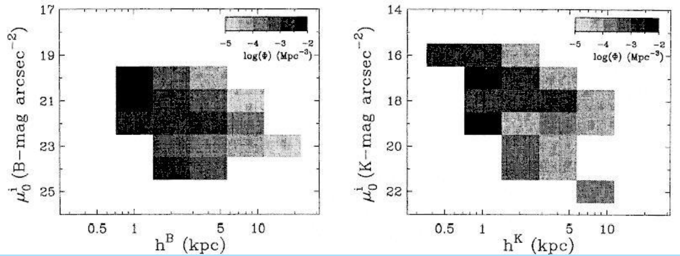

From a weighing with the total luminosity it can be estimated that high surface brightness galaxies probably provide the majority of the luminosity density in the universe.

Elliptical galaxies

Luminosty distributions

Elliptical galaxies usually conform to the $R^{1/4}$-law and look smooth and regular.

NGC 3379 has been used as a prototype and standard for surface photometry[a].

[a] G. de Vaucouleurs & M. Capaccioli, Ap.J.Suppl. 40, 699 (1979)

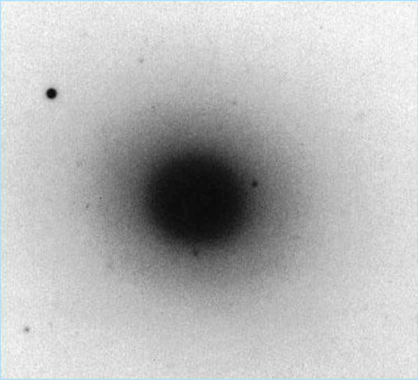

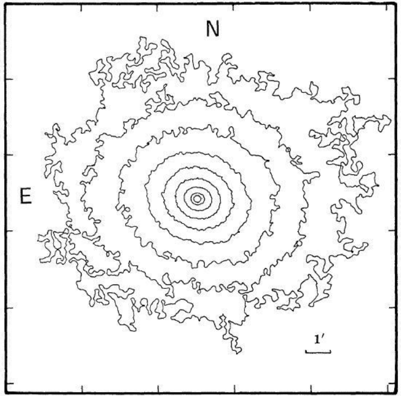
N
E
1′

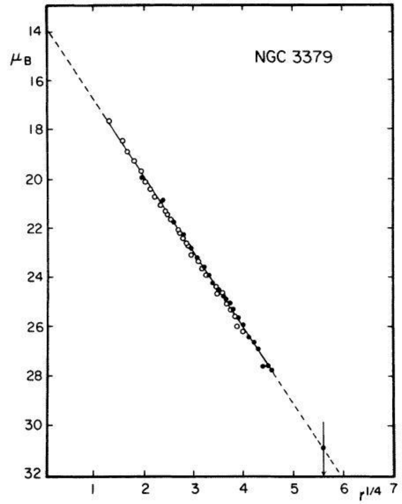
NGC 3379
μ_B
14
16
18
20
22
24
26
28
30
32
1
2
3
4
5
6
7
$r^{1/4}$

Detailed study shows that the isophotal structure of ellipticals is usually much more complicated.

In particular there are isophote twists and deviations from ellipticity.

The latter are described by parameters $a(i)$.
These describe the deviations from pure ellipses in multiplicity i[28].
These are derived from Fourier analysis of the isophote shapes relative to the best fitting ellipse.

By definition (because of the ellipse fit) $a(i) = 0$ for $i = 0, 1, 2$.

[28] R. Bender, S. Döbereiner & C. Möllenhoff, A.&A.Suppl. 74, 385 (1988)

The most interesting is $a(4)$, which is negative for "boxy" isophotes and positive for "disky" isophotes.

Here are some examples of non-zero parameters $a(4)$.

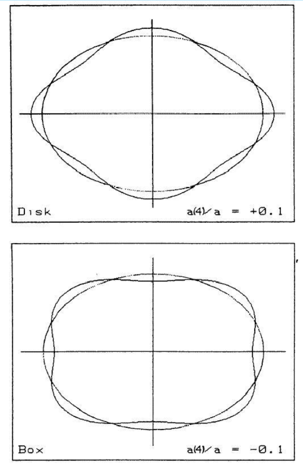

We will now look at fits in a boxy galaxy.

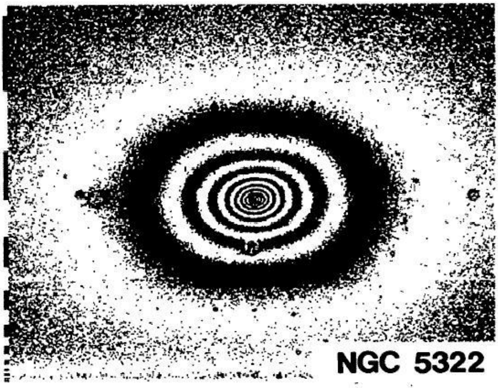

FIGURE 7. — R-image of NGC 5322, an elliptical galaxy with box-shaped isophotes $(a(4)/a \sim -0.01)$.

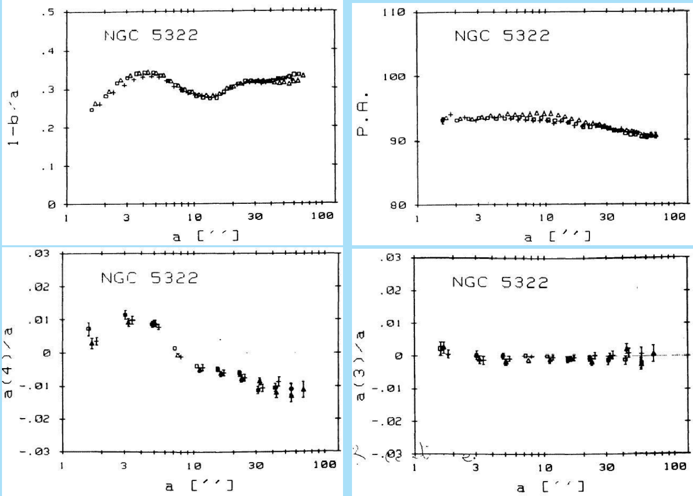
NGC 5322
1−b/a
a [″]
NGC 5322
P.A.
a [″]
NGC 5322
a(4)/a
a [″]
NGC 5322
a(3)/a
a [″]

And here are fits a disky galaxy.

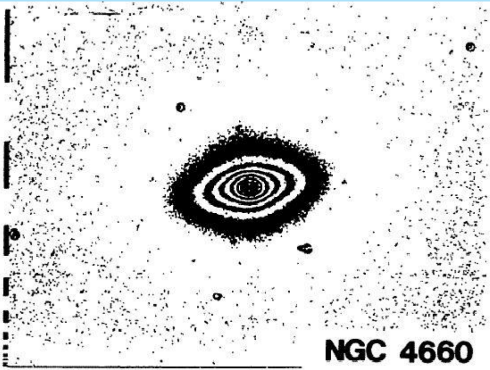

FIGURE 6. — R-image of NGC 4660, an elliptical galaxy with a disk-component in the isophotes $(a(4)/a \sim +0.03)$.

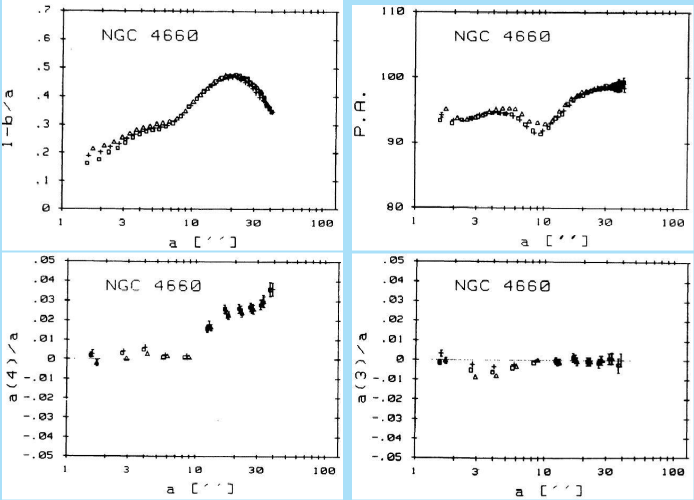
NGC 4660
1-b/a
a [″]
NGC 4660
P.A.
a [″]
NGC 4660
a(4)/a
a [″]
NGC 4660
a(3)/a
a [″]

The global $a(4)$ parameter for a sample of galaxies does not correlate with effective radius or integrated luminosity[29].

However, galaxies with strong radio emission or X-ray halo's are almost always boxy.

It has been suggested that "boxyness" results from interactions.

[29] R. Bender, P. Surma, S. Döbereiner, C. Möllenhoff & R. Madejsky, A.&A. 217, 35 (1989)

Color gradients

Important for formation models is the correlation of color gradients with structural and dynamical properties.

Color gradients usually are defined as the change in color index in magnitudes per decade in radius or
$\bigtriangledown(B-V) = \Delta(B-V)/\Delta(\log r)$.

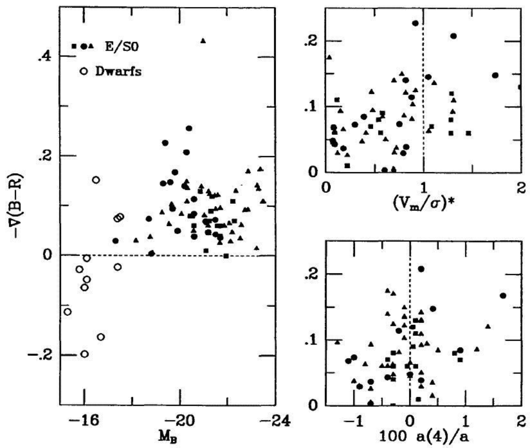
E/S0
Dwarfs
.4
.2
0
−.2
−∇(B−R)
−16
−20
−24
M_B
.2
.1
0
0
1
2
$(V_m/\sigma)^*$
.2
.1
0
−1
0
1
2
100 a(4)/a

The property $(V_{\mathrm{m}}/\sigma)^{*}$ is normalised to unity for an isotropic oblate rotator.

- Ellipticals have significant color gradients. The light becomes redder towards the center.
- However, dwarf spheroidals have inverse gradients. This may be due to recent star formation.
- Anisotropic galaxies have smaller gradients.
- Also boxy galaxies tend to have smaller gradients.
- There is no strong correlation between the strength of the color gradient and the luminosity or velocity dispersion.

Abundance gradients

Elliptical galaxies and **bulges** have color gradients (become bluer with radius).

This is due to metallicity changes.

For a low [Fe/H] in an old population:

- The effective temperature of the giant branch is higher
- There is less line-blanketing
- The horizontal branch is more extended towards the blue.

The relation between color and metallicity can be calibrated using the integrated light of Galactic globular clusters.

The range in (U-B),(B-V) in bulges is roughly that in globular clusters.

So the range in metallicity in bulges is 1 - 2 dex in [Fe/H]. }

There is such a pronounced color gradient in the bulge of NGC 7814[30]

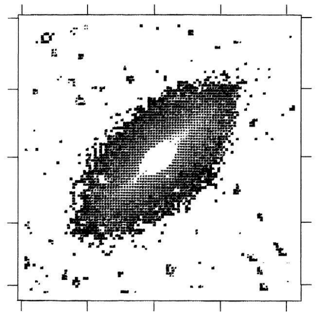

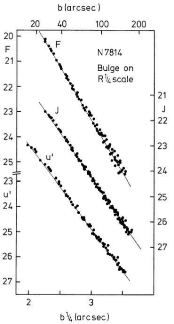

$$\mu_{U'} = 14.87 + 3.32 b^{1/4}$$
$$\mu_{J\,\mathrm{opt}} = 13.72 + 3.55 b^{1/4}$$
$$\mu_V = 13.08 + 3.75 b^{1/4}$$
$$\mu_F = 10.70 + 4.20 b^{1/4}$$
$$\mu_J = 9.19 + 4.36 b^{1/4}$$
$$\mu_K = 8.07 + 4.43 b^{1/4}$$

[30] P.C. van der Kruit & L. Searle, A.&A. 110, 79 (1982); R.J. Wainscoat, A.R. Hyland & K.C. Freeman, Ap.J. 348, 85 (1990)